J Physiol 595.21 (2017) pp 6703–6718

The Journal of Physiology

Synaptic excitation by climbing fibre collaterals in the cerebellar nuclei of juvenile and adult mice

Marion Najac and Indira M. Raman

Department of Neurobiology, Northwestern University, Evanston, IL, USA

Key points

- The inferior olive sends instructive motor signals to the cerebellum via the climbing fibre projection, which sends collaterals directly to large premotor neurons of the mouse cerebellar nuclei (CbN cells).
- Optogenetic activation of inferior olivary axons *in vitro* evokes EPSCs in CbN cells of several hundred pA to more than 1 nA.
- The inputs are three-fold larger at younger ages, 12 to 14 days old, than at 2 months old, suggesting a strong functional role for this pathway earlier in development.
- The EPSCs are multipeaked, owing to burst firing in several olivary afferents that fire asynchronously.
- The convergence of climbing fibre collaterals onto CbN cells decreases from ∼40 to ∼8, which is consistent with the formation of closed-loop circuits in which each CbN neuron receives input from 4–7 collaterals from inferior olivary neurons as well as from all 30–50 Purkinje cells that are innervated by those olivary neurons.

Abstract The inferior olive conveys instructive signals to the cerebellum that drive sensorimotor learning. Inferior olivary neurons transmit their signals via climbing fibres, which powerfully excite Purkinje cells, evoking complex spikes and depressing parallel fibre synapses. Additionally, however, these climbing fibres send collaterals to the cerebellar nuclei (CbN). *In vivo* and *in vitro* data suggest that climbing fibre collateral excitation is weak in adult mice, raising the question of whether the primary role of this pathway may be developmental. We therefore examined climbing fibre collateral input to large premotor CbN cells over development by virally expressing channelrhodopsin in the inferior olive. In acute cerebellar slices from postnatal day (P)12–14 mice, light-evoked EPSCs were large (> 1 nA at −70 mV). The amplitude of these EPSCs decreased over development, reaching a plateau of ∼350 pA at P20–60. Trains of EPSCs (5 Hz) depressed strongly throughout development, whereas convergence estimates indicated that the total number of functional afferents decreased with age. EPSC waveforms consisted of multiple peaks, probably resulting from action potential bursts in single collaterals and variable times to spike threshold in converging afferents. Activating climbing fibre collaterals evoked well-timed increases in firing probability in CbN neurons, especially in younger mice. The initially strong input, followed by the decrement in synaptic strength coinciding with the pruning of climbing fibres in the cerebellar cortex, implicates the climbing fibre collateral pathway in early postnatal development. Additionally, the persistence of substantial synaptic input at least to P60 suggests that this pathway may function in cerebellar processing into adulthood.

(Received 5 May 2017; accepted after revision 8 August 2017; first published online 10 August 2017)
Corresponding author I. M. Raman: Department of Neurobiology, 2205 Tech Drive, Northwestern University, Evanston, IL 60208, USA. Email: i-raman@northwestern.edu

Abbreviations aCSF, artificial cerebrospinal fluid; CbN, cerebellar nuclei; cfEPSC, climbing fibre EPSC; cfcEPSC, climbing fibre collateral EPSC; ChR2, channelrhodopsin; CPP, (RS)-3-(2-carboxypiperazin-4-yl)-propyl-1-phosphonic acid; DNQX, 6,7-dinitroquinoxaline-2,3-dione; IO, inferior olive; mfEPSC, mossy fibre EPSC; P, postnatal day; PSTH, post-stimulus time histogram.

DOI: 10.1113/JP274598

Introduction

The cerebellum receives sensory and motor information conveyed by mossy fibres from several brain regions, as well as teaching and/or error signals conveyed via climbing fibres from the inferior olive (IO) (Marr, 1969; Albus, 1971; Gilbert & Thach, 1977; García & Mauk, 1998, Medina *et al.* 2002). Each climbing fibre makes extensive contacts onto Purkinje cells of the cerebellar cortex, evoking giant EPSCs that trigger complex spikes and induce synaptic plasticity. In addition, however, climbing fibre collaterals innervate the cerebellar nuclei (CbN), where they form smaller, more conventional synapses on the dendrites of CbN neurons (Chan-Palay, 1977; Wiklund *et al.* 1984; van der Want & Voogd, 1987; De Zeeuw *et al.* 1997; Sugihara *et al.* 1999, 2001). The major role of olivocerebellar signals in motor learning and error correction via the cerebellar cortex raises the question of how these olivary signals affect cerebellar output neurons directly via climbing fibre synapses in the CbN.

These synapses have been explored repeatedly *in vivo*, although identifying the functional influence of climbing fibre collaterals on CbN cells has been complicated by the difficulties of selective, controlled activation of this pathway. For example, early *in vivo* studies recorded small, short-latency EPSPs in the CbN after electrical stimulation of the IO (Eccles *et al.* 1974), although these responses might have resulted either from direct inputs or from antidromic activation of mossy fibres that also projected to the olive. Efforts to isolate the effects of direct inputs have relied on anatomical evidence that inferior olivary neurons, Purkinje cells and CbN cells form closed loops (Voogd & Bigaré, 1980; Ruigrok & Voogd, 2000; Apps & Hawkes, 2009; Sugihara, 2011; Cerminara *et al.* 2013), suggesting that complex spikes in Purkinje cells should coincide with climbing fibre collateral-mediated excitation followed by Purkinje-mediated inhibition in CbN neurons. Consistent with this prediction, in an *in vitro* brainstem-cerebellum preparation from adult guinea pigs, harmalin-induced oscillations in the IO occasionally elicited EPSP–IPSP sequences in CbN neurons (Llinás & Mühlethaler, 1988). Similarly, in 24% of simultaneous *in vivo* recordings from adult rats, spontaneous complex spikes in Purkinje cells coincided with an excitation–inhibition sequence in CbN neurons (Blenkinsop & Lang, 2011; Tang *et al.* 2016). Although these results demonstrate direct, functional synapses between climbing fibre collaterals and CbN cells in closed loops with Purkinje–CbN afferents, evidence for such connections is noticeably rare. Indeed, optogenetic activation of Ptf1a-expressing inferior olivary neurons *in vivo* found that inhibition generally overwhelmed excitation; in the same study, light-evoked EPSCs in CbN neurons *in vitro* had extremely small amplitudes that rarely affected CbN cell firing (Lu *et al.* 2016).

What contribution, if any, climbing fibre collaterals make to cerebellar signalling thus remains uncertain. One proposal is that they contribute to the wiring of circuits during development (Lang *et al.* 2017). Indeed, anatomical studies revealed a larger number of collaterals and swellings in the nuclei of two postnatal day (P)4–6 inferior olivary axons relative to adult axons (Sugihara, 2005). Therefore, we measured the synaptic properties of identified climbing fibre collaterals and their evolution during development by selectively expressing channelrhodopsin (ChR2) in inferior olivary neurons of mice and recording light-evoked EPSCs in large premotor CbN neurons at different ages during postnatal development. The data demonstrate that, in the first 2 weeks of life, olivary-dependent synaptic currents in CbN cells results from many convergent climbing fibre collaterals. These afferents collectively provide strong synaptic input that can alter firing. Their strength declines as mice develop into adulthood.

Materials and methods

Ethical approval

All procedures conformed to institutional and NIH guidelines and were approved by the Northwestern University IACUC. Animals were killed using methods consistent with the recommendations of the Panel on Euthanasia of the American Veterinary Medical Association. The research complies with the policies of *The Journal of Physiology* (Grundy, 2015). Mice were housed in Northwestern's accredited animal care facility with *ad lib.* access to food and water.

Viral injections

P1 and P21–23 C57BL6 mice (Jackson Laboratories, Bar Harbor, ME, USA; Charles River Laboratories, Wilmington, MA, USA) of either sex received injections into the IO for optogenetic labelling of axons with the ChR2-expressing virus AAVDJ-CaMKIIa-hChR2 (H134R)-EYFP/mCherry (Gene Vector and Virus Core, Stanford University, Stanford, CA, USA) (Nguyen-Vu *et al.* 2013). Because mossy fibres and inferior olivary axons enter the cerebellum during the embryonic stage (Rahimi-Balaei *et al.* 2015), their sources in the brainstem can be targeted even at P1. To allow entry of the injection pipette, P1 mice were anaesthetized by isoflurane inhalation and a slight incision was made in the skin and skull with a 28 G needle and P21–23 mice were anaesthetized with ketamine/xylazine (90 and 3 mg kg^{-1}, I.P.) and craniotomized (Najac & Raman, 2015). The depth of anaesthesia was checked by toe pinch every 15 min. The tip of the micropipette was dipped into 300 nL of virus containing solution that was taken up by capillary

action. The pipette was positioned stereotaxically and approximately half of the virus-containing solution (i.e. 100 to 200 nL) was applied through a Picospritzer. In P21–23 animals, stereotaxic positions were as described in Najac and Raman (2015). The virus was injected at two sites (anteroposterior: 5.4 and 5.75 mm) along the rostrocaudal axis of the IO (lateral: 400–450 μm; depth: 6.4–6.6 mm). In P1 pups, the confluence point of the superior sagittal and transverse sinuses served as a reference. The head orientation was adjusted so that the head surface 2.5 mm caudally was 0.95 mm below this reference point. One injection was made at the co-ordinates (from reference point): 2.5 mm caudal, 0.3 mm lateral (left) and 5.3–4.9 mm deep.

P21–23 mice were given BuprenorphineSR (ZooPharm, Laramie, WY, USA) as an analgesic. Injected mice were kept on a warming pad to maintain body temperature when the surgery was performed and until recovery from anaesthesia was complete. Mice were housed in cages containing an oblique running wheel to provide them with an opportunity to engage in co-ordinated movement and motor learning. At least 11 days were allowed for ChR2 expression before anatomical or physiological experiments. Experiments were performed up to 60 days following injection.

Histology

To visualize EYFP or mCherry labelling by the virus, mice were anaesthetized with pentobarbital (60 mg kg^{-1}, I.P.). Anaesthesia was confirmed by the lack of response to toe pinch. Mice were then perfused with 4% paraformaldehyde. Brains were stored overnight in paraformaldehyde, and rinsed with PBS. Sections of fixed tissue (50–100 μm) were cut and mounted. Confocal images were taken with an SP5 confocal microscope (Leica Microsystems, Wetzlar, Germany).

Electrophysiology

Slices were prepared as described in Najac and Raman (2015). Mice were anaesthetized with isoflurane until unresponsive to toe pinch and then decapitated. Cerebella were removed and transferred into oxygenated (95% O_2/5% CO_2) artificial cerebrospinal fluid (aCSF) (35–36°C) containing (in mM): 123 NaCl, 3.5 KCl, 1.5 $CaCl_2$, 1 $MgCl_2$, 26 $NaHCO_3$, 1.25 NaH_2PO_4 and 10 glucose. Coronal or parasagittal slices (270 μm) were cut on a VT1200 vibratome (Leica Microsystems, Wetzlar, Germany), incubated for 30–40 min at 34–36°C in oxygenated aCSF and then maintained at room temperature until recordings were made.

Slices were bathed in oxygenated aCSF at 33–34°C (perfusion rate 2.5–3 mL min^{-1}) in a recording chamber on the stage of a Examiner D1 microscope (Zeiss) with a TILL Photonics imaging system (FEI Life Science, Munich, Germany). Slices were examined for the efficacy of viral infection of axons by inspection of the cerebellar cortex. If fluorescent fibres were evident in the contralateral molecular layer (i.e. where climbing fibres innervate Purkinje cell dendrites), the injection was considered to have effectively targeted the IO. If fluorescent fibres were evident in the ipsilateral granule cell layer (i.e. where mossy fibres innervate granule cells), the injection was considered as having been mistargeted to brainstem regions giving rise to mossy fibres and the data were interpreted accordingly. Fluorescent labelling of both the contralateral molecular and granule layers was not observed.

Recordings were made with a Multiclamp 700B amplifier with pClamp software (Molecular Devices, Sunnyvale, USA). Climbing fibres and climbing fibre collaterals were identified by fluorescence and large premotor CbN cells were identified by somatic diameters of 20–25 μm. As a result of small differences in the size and shape of neonates, the portion of the IO that was infected by the viral injection could vary across P1 mice. Different regions of the IO innervate different portions of the cerebellar nuclei, forming olivocerebellar modules (Ruigrok & Voogd, 2000). Therefore, CbN cells in slices were selected for recording only if they were in the vicinity of fluorescence-labelled terminals, which indicated that the corresponding module(s) in the olive had successfully incorporated virus. All cells in the present study were located in the interpositus or lateral nuclei. The study incorporated data from 53 mice injected at P1 and 11 mice injected at P21–23, and so variations in injection site resulting from intrinsic variability in P1 mice are probably equivalently represented in the different age groups studied.

For whole-cell voltage clamp recordings, patch pipettes (2–3 MΩ) contained (in mM): 120 $CsMeSO_3$, 14 Tris-creatine phosphate, 12 sucrose, 10 Hepes, 4 Mg-ATP, 4 TEA-Cl, 3 NaCl, 2 $MgCl_2$, 1.2 QX314, 1 EGTA and 0.3 Tris-GTP (buffered to pH 7.32 with 14 mM CsOH, ~290 mOsm; measured uncorrected junction potential of 4 mV). Access resistances were 8.2 ± 0.2 MΩ (n = 112) in large CbN cells and 9.5 ± 0.7 MΩ (n = 10) in Purkinje cells and were not compensated, although they were monitored for stability throughout each experiment. Cell-attached recordings were made either before breaking in for voltage clamp recording or in loose-cell attached mode, in which case patch pipettes (5–7 MΩ) were filled with a Hepes-based solution containing (in mM): 145 NaCl, 10 Hepes, 3.5 KCl, 1.5 $CaCl_2$ and 1 $MgCl_2$ (buffered to pH 7.36 with NaOH). Recordings were made at 33–34°C, which is a temperature range that provided more stability and longer cell survival than 36–37°C at the same time as being close to physiological temperature. Assuming a Q10 of 3, all rates reported can be scaled by 1.4 to estimate physiological values.

Optogenetic stimulation

To stimulate a maximal number of climbing fibres and their collaterals, 1–2 ms blue light pulses (Polychrome; TILL Photonics, Gräfelfing, Germany) were delivered through the microscope objective. For local and graded stimulations, 1–2 ms blue LED light pulses (Doric, Quebec, Canada) were targeted near the recorded cell through a cannula-coupled optic fibre (Thorlabs, Newton, NJ, USA) (maximum of 350 lux).

Drugs

Where indicated, 2–10 μM 6,7-dinitroquinoxaline-2,3-dione (DNQX), 10 μM (RS)-3-(2-carboxypiperazin-4-yl)-propyl-1-phosphonic acid (CPP) or 10 μM gabazine [SR95531; 6-imino-3-(4-methoxyphenyl)-1(6H)-pyridazinebutanoic acid hydrobromide] was added to aCSF to block AMPA, NMDA or $GABA_A$ receptors. Climbing fibre EPSCs in Purkinje cells were recorded in the presence of 2–5 μM of DNQX to decrease the EPSC amplitude enough to prevent unclamped action potentials. All chemicals were from Sigma-Aldrich (St Louis, MO, USA), except DNQX, CPP and SR95531 (Tocris, Bristol, UK).

Data analysis

Voltage clamp data were filtered offline at 1–2 kHz and cell-attached data at 5–10 kHz. All data were analysed with IGOR-Pro (Wavemetrics, Portland, OR, USA) with NeuroMatic packages and Axograph (Axograph Scientific, Berkeley, CA, USA). Latencies were measured at 5% of EPSC maximum amplitude and jitter was defined as the standard deviation of the latency. Charge transfer was measured over 10 ms following EPSC onset. EPSC characteristics were measured from averages (three to 20 repeated stimuli except in Fig. 1 where measurements were made on individual records and then averaged.) EPSC decays were fitted with a sum of two exponentials to calculate a weighted time constant, $\tau = A_1{}^*\tau_1 + A_2{}^*\tau_2$, where A_1 and A_2 are the percentage contributions of the fast and slow exponentials of the fits, which decay with time constant τ_1 and τ_2, respectively. For cell-attached recordings, the duration of increase in firing rate was estimated from single-exponential fits to post-stimulus time histograms (PSTHs), constructed with 5 ms bins.

Statistical analysis

Data are presented as the mean ± SEM. Statistical significance was assessed with Wilcoxon–Mann–Whitney two-sample rank tests for unpaired data (IGOR-Pro), two-tailed *t* tests for paired data (GraphPad, La Jolla, CA, USA) or ANOVAs for data sets with more than two variables (SPSS Statistics; IBM, Armonk, NY, USA) and *P* values are reported.

Results

Labelling climbing fibre collaterals for optogenetic stimulation

To test how the activity of climbing fibre collaterals affects neurons of the cerebellar nuclei, we introduced ChR2 into the cells from which they originate. AAVDJ-CaMKIIa-hChR2(H134R)-EYFP/mCherry virus was injected into the IO of newborns (P1) and weanling mice (P21–23) to express EYFP or mCherry coupled to ChR2 in IO axons (Fig. 1*Aa*). When recordings were made 11–60 days later in slices, fluorescence was visible in climbing fibres in the cerebellar cortex (Fig. 1*Ab* and *Ac*) and in climbing fibre collaterals in the CbN (Fig. 1*Ad*). The restriction of most fluorescent fibres to the contralateral side is in agreement with anatomical studies (Wiklund *et al.* 1984; van der Want & Voogd, 1987; De Zeeuw *et al.* 1997; Sugihara *et al.* 1999, 2001) and confirms that labelling resulted from expression in IO neurons rather than along the pipette track. Occasionally, a few ipsilateral mossy fibres were labelled.

Climbing fibre collateral synaptic inputs onto CbN cells change over postnatal development

We first confirmed that IO axons had successfully incorporated ChR2 by recording from Purkinje cells in cerebellar slices from mice ≥ P20 (weanlings and adults injected at P1). Optogenetic stimulation was delivered through the microscope objective to maximize the number of afferents activated. In Purkinje cells postsynaptic to fluorescent terminals, 1–2 ms blue light pulses elicited climbing fiber EPSCs (cfEPSCs), confirming that inferior olivary axons had successfully expressed ChR2 (Fig. 1*B*). These Purkinje cell cfEPSCs exceeded several hundred picoamps at −70 mV (0.35–2.5 nA, $n = 7$), even when 2–5 μM DNQX was added to reduce their amplitudes. We therefore recorded the responses from large CbN cells that were surrounded by fluorescent climbing fibre collateral terminals (in aCSF without DNQX present). In mice ≥ P20, climbing fiber collateral EPSCs (cfcEPSCs) amplitude was −351 ± 40 pA at −70 mV ($n = 49$) (Fig. 1*B* and *C*). In juvenile mice, cfcEPSC amplitudes were even larger. Plotting cfcEPSC amplitude as a function of age showed a fairly rapid decrement in response magnitude between P12 and P20, which then stabilized at older ages. For quantification, we subdivided the data into three categories: P12–14, which had the largest responses; P15–19, which had intermediate responses; and ≥ P20, which had stable responses up to P60 (the oldest ages tested here). At P15–19, cfcEPSC amplitude was significantly

larger than in older mice (−646 ± 101 pA, $n = 30$, $P = 0.015$). At P12–14, cfcEPSCs were greater still, exceeding −1 nA in the majority of cells (1.2 ± 0.2 nA, $n = 13$, $P = 0.0001$) (Fig. 1*B* and *C*), which is more than three times larger than the oldest group tested. These data suggest that the total synaptic strength of climbing fibre collaterals to CbN cells is high in the second week of life and then decreases as postnatal development progresses.

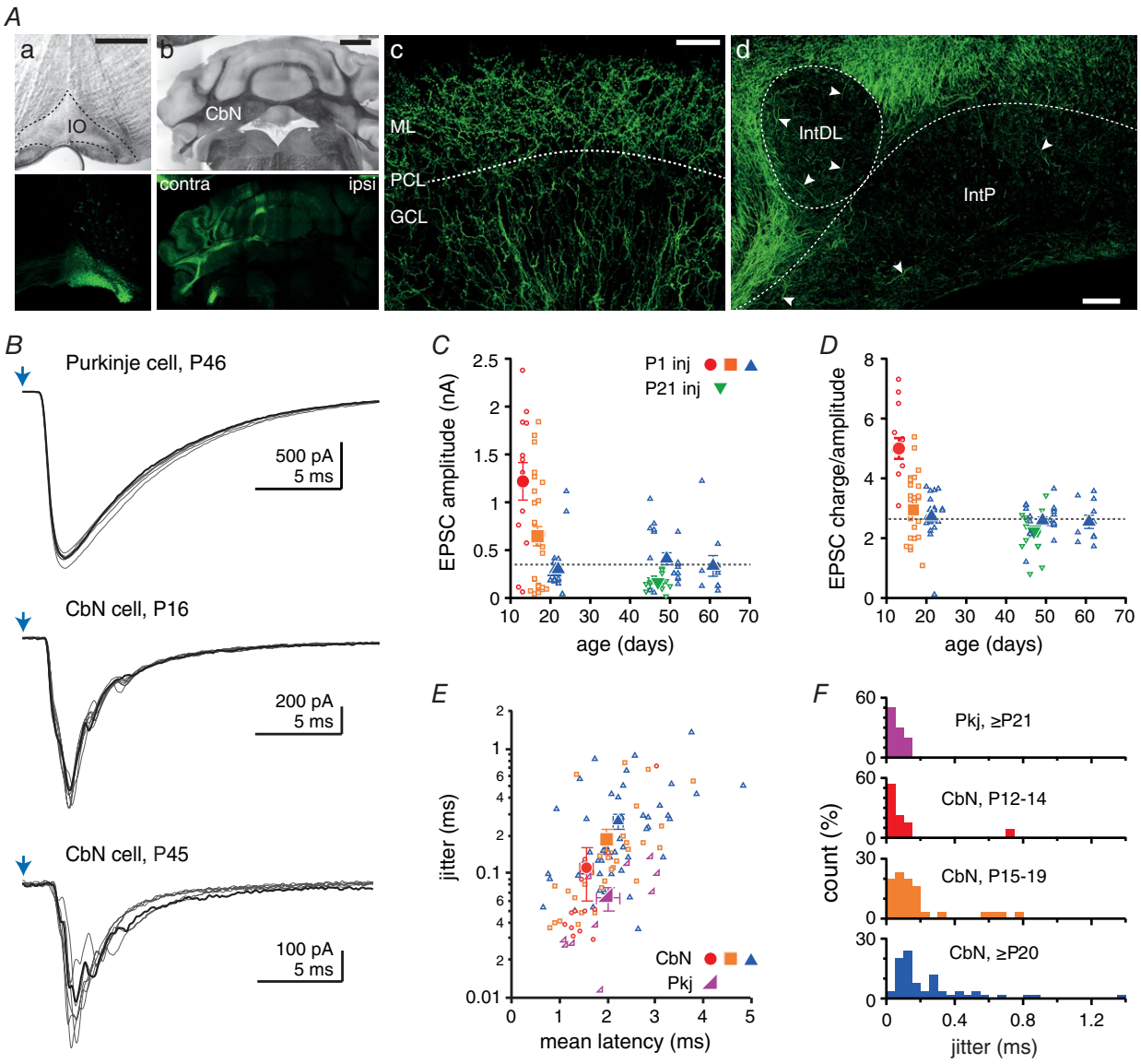

Figure 1. Light-evoked cfcEPSCs in large CbN neurons change during postnatal development
A, coronal sections of the brainstem (*Aa*) and cerebellum (*Aa–Ad*) after viral injection into the IO. *Aa* and *Ab*, Expression in IO neurons results in anterograde labelling of climbing fibres (CFs) in the contralateral cerebellum (top, differential interference contrast; bottom, Z-stacks of confocal images). *Ac*, Z-stacks of confocal images showing labelled CFs in the cerebellar cortex. ML, molecular layer. PCL, Purkinje cell layer. GCL, granule cell layer. *Ad*, Z-stacks of confocal images showing climbing fibre collaterals (arrowheads) in the posterior interpositus nucleus (IntP) and the dorsolateral horn of the interpositus nucleus (intDL). Scale bars: (*Aa*) 500 μm, (*Ab*) 1 mm, (*Ac*) 50 μm and (*Ad*) 100 μm. *B*, light-evoked EPSCs in a Purkinje cell (cfEPSCs, top) and CbN neurons at different ages (cfcEPSC, middle and bottom). Purkinje cell cfEPSCs were recorded in the presence of 5 μM DNQX. One example trace of six is highlighted. Blue arrow, stimulation time. *C*, maximal cfcEPSC amplitude *vs*. age in CbN cells. After P1 injection: red circles, P12–14; orange squares, P15–19; blue triangles, P20–62. After P21 injection: green triangles, P44–50. Filled symbols are mean data. Dashed line, steady-state amplitude in adults. *D*, cfcEPSC charge over amplitude ratio *vs*. age. Same symbols as in (*C*). *E*, EPSC jitter (SD latency) *vs*. EPSC mean latency in CbN neurons at various ages (symbols as in *C*) and Purkinje cells (≥ P21, magenta right triangle). *F*, distribution of EPSC jitter in CbN neurons and Purkinje cells. Same data as in (*E*).

Indeed, the data may underestimate the age-dependent decrement because all mice were injected at P1 and expression of virally expressed genes tends to increase with age (Miyashita *et al.* 2013). Alternatively, because the expression of ChR2 for > 40 days can induce cellular degeneration in some preparations (Miyashita *et al.* 2013), the longer expression period in older mice might have damaged axons and produced artefactually smaller responses. When injections were made at P21–23, however, cfcEPSCs at P40–50 were only −166 ± 20 pA ($n = 16$) (Fig. 1*C*), which is smaller than with P1 injections, suggesting that the lower response magnitudes at older ages were not simply an outcome of longer incubation times. Regardless of injection age, the cfcEPSC amplitudes measured here at P20–60 were several-fold larger than those reported previously 3–6-month-old mice (−7 pA) in response to optogenetic stimulation of Ptf1a-expressing IO cells (Lu *et al.* 2016).

The cfcEPSCs also had characteristic waveforms. Unlike cfEPSCs in Purkinje cells, which were monophasic (e.g. Dittman *et al.* 1998; Wadiche & Jahr, 2001), cfcEPSCs at all ages were composite, consisting of multiple peaks (2.9 ± 0.1 detectable peaks per stimulation, $n = 86$) (Fig. 1*B*). As a result of these multiple events, the peak amplitude of cfcEPSCs might not provide the best estimate of synaptic strength. We therefore quantified the charge transfer of cfcEPSCs and found that it also decreased with age (one-way ANOVA, $F_{2,89} = 36$, $P < 0.0001$): the charge transfer was significantly larger at P12–14 than at P15–19 (6.9 ± 1.3 nC, $n = 13$ *vs.* 2.3 ± 0.4 nC, $n = 30$, $P = 0.0007$) or at ≥ P20 (0.9 ± 0.1 nC, $n = 49$, $P < 0.0001$). The charge transfer decreased with development even more steeply than did amplitude, leading to a charge-over-amplitude ratio that was twice as large at P12–14 than at ≥ P20 (5.3 ± 0.3 *vs.* 2.5 ± 0.6, $P < 0.0001$) (Fig. 1*D*). These data demonstrate that, in addition to having larger mean amplitudes, cfcEPSCs in juveniles are longer relative to those in weanlings and adults. This prolongation might result from dispersion of release events and/or the slower kinetics of postsynaptic receptors, either of which could contribute to increasing the efficacy of transmission.

In addition to changes in magnitude over development, cfcEPSCs showed changes in timing. The latency of cfcEPSCs increased with age (one-way ANOVA, $F_{2,89} = 3.7$, $P = 0.03$), being longer at ≥ P20 (2.2 ± 0.1 ms, $n = 49$) than at P12–14 (1.6 ± 0.1 ms, $n = 13$; $P = 0.001$). Repeated stimulation demonstrated that cfcEPSC timing also tended to become more variable, as quantified by the SD on the latency (i.e. jitter) (one-way ANOVA, $F_{2,89} = 2.7$, $P = 0.07$), which was smaller at P12–14 (0.11 ± 0.05 ms, $n = 13$) than at ≥ P20 (0.26 ± 0.04 ms, $n = 49$; $P < 0.0001$) (Fig. 1*E* and *F*). Release is thus less well-timed at older ages. For comparison, we examined the latency of cfEPSCs in Purkinje cells. Although cfEPSC latencies at ≥ P20 (2.0 ± 0.2 ms) were similar to those of cfcEPSCs ($P = 0.5$), they were less variable (jitter, 0.06 ± 0.01 ms, $n = 10$, $P < 0.0001$) (Fig. 1*E* and *F*). The difference in variance is consistent with ultrastructural studies showing that Purkinje cells each receive numerous contacts from a single climbing fibre, whereas large CbN cells receive single *en passant* contacts, presumably from several different climbing fibre collaterals (Chan Palay, 1977).

Short-term depression of climbing fibre collaterals synaptic inputs

Next, we investigated the short-term plasticity of cfcEPSCs, to test the extent to which they resemble the primary climbing fibre branches in the cerebellar cortex, which are subject to strong synaptic depression (Konnerth *et al.* 1990; Dittman & Regehr, 1998). Because inferior olivary neurons tend to fire at rates between 0.1 and 10 Hz in many mammals, including mice (Thach, 1968; Armstrong & Rawson, 1979; Llinás & Sasaki, 1989; Lang *et al.* 1999; Khosrovani *et al.* 2007), we recorded cfcEPSCs evoked by 5 Hz, 1 s trains (Fig. 2*A*). In a few mice, a mistargeting of injection was evident as an absence of contralateral fluorescent climbing fibres in the cerebellar cortex as well as the presence of mossy fibres labelled both ipsilaterally and contralaterally. Recordings of light-evoked mossy fibre EPSC (mfEPSC) from these animals were analysed for comparison.

To quantify the depression of synaptic transmission in the nuclei, we calculated the paired-pulse amplitude ratio as the current elicited by the second light pulse relative to the first at −70 mV ($EPSC_{2/1}$) (Fig. 2*B*). Even at a frequency as low as 5 Hz, the paired-pulse ratio for cfcEPSCs was approximately half, and was not affected by age (one-way ANOVA, $F_{2,80} = 0.23$, $P = 0.98$; P12–14, 0.52 ± 0.03, $n = 13$; P15–19, 0.51 ± 0.04, $n = 25$; ≥ P20, 0.51 ± 0.03, $n = 45$) (Fig. 2*C* and *D*). By contrast, mfEPSCs depressed much less at 5 Hz (P15–19 $mfEPSC_{2/1}$ amplitude ratio, 0.74 ± 0.03, $n = 9$, $P = 0.0005$) and the amplitude of the first mfEPSC was half that of cfcEPSCs at the same age (149 ± 31 pA, $P = 0.03$) (Fig. 2*B*–*D*). The amplitude ratio of the last to the first current ($cfcEPSC_{5/1}$) was similar to $cfcEPSC_{2/1}$ in P12–14 mice (0.45 ± 0.03, $P = 0.064$) but became even smaller with development (P15–19, 0.39 ± 0.03, $P < 0.0001$; ≥ P20, 0.36 ± 0.03, $P < 0.0001$). The reduction in cfcEPSC amplitude over the first postnatal weeks therefore probably does not result from a decrease in release probability, which remains high. Along with eliciting fast cfcEPSCs, trains of stimuli sometimes activated a small, slow inward current at −70 mV (−35 ± 6 pA; monoexponential τ decay, 660 ± 65 ms, $n = 6$) (Fig. 2*A*). This current was present in 5/13 (38%) cells at P12–14 and 1/25 (4%) cells at P15–19 and was absent from all cells at ≥ P20 ($n = 43$). It is consistent with an mGluR1/5-dependent current (Mercer *et al.* 2016) but could also result from other neuromodulators

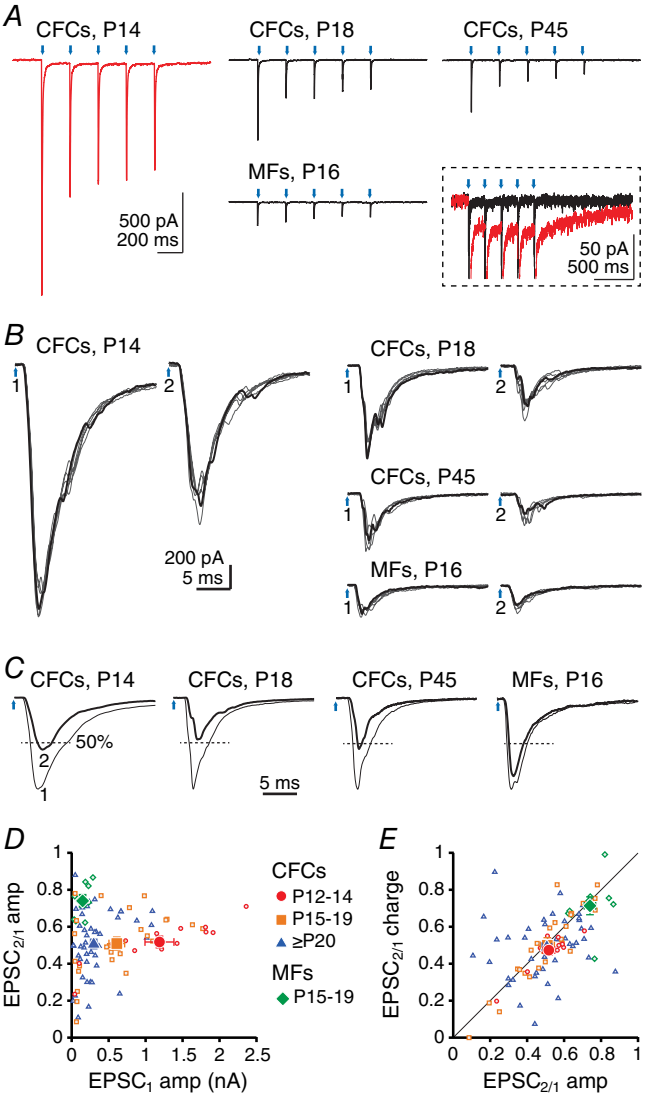

Figure 2. cfcEPSCs depress strongly in CbN neurons
A, averaged EPSCs evoked by a 5 Hz train of light pulses at different ages with ChR2 expressed in climbing fibre collaterals (CFCs) or mossy fibres (MFs). Red, cfcEPSC at P14. Black, all other records. Blue arrows, stimulation times. Inset, all traces from A, magnified and superimposed to illustrate the small-amplitude slow inward current (red, P14 trace). *B*, enlarged traces of responses to the first two stimuli of the 5 Hz train (200 ms interval) at different ages with ChR2 expressed in CFCs or in MFs. One example trace of six is highlighted. Blue arrows 1 and 2, stimulation times. *C*, superimposed normalized averages for $EPSC_1$ and $EPSC_2$. $EPSC_2$ is highlighted. Dashed lines indicate 50% of $EPSC_1$ amplitude. *D*, paired-pulse ratio of EPSC amplitude ($EPSC_2/EPSC_1$ peak) *vs.* $EPSC_1$ amplitude for CFC or MF stimulation following viral injection at P1. For cfcEPSCs: red circles, P12–14; orange squares, P15–19; blue triangles, P20–62. For mfEPSCs: green lozenges, P15–19. Filled symbols, mean data. *E*, paired-pulse ratio of EPSC charge *vs.* paired-pulse ratio of EPSC amplitude. Same symbols as in (*C*). Filled circle, square and triangle overlap and obscure one another.

and, because of its rarity, it was not investigated further.

For comparison with other studies of depression of electrically evoked CbN EPSCs, we also elicited 20 Hz trains with optogenetic stimulation of either climbing fibre collaterals or mossy fibres. At this frequency, the paired-pulse ratio was 0.51 ± 0.05 for cfcEPSCs ($n = 6$, P12–17) and 0.85 ± 0.11 for mfEPSCs ($n = 7$, P15–19) and the steady-state ratio at the end of the 1 s train was 0.14 ± 0.03 for cfcEPSCs and 0.41 ± 0.06 for mfEPSCs. This value for mfEPSCs is in good agreement with measurements from electrically evoked EPSCs in CbN cells in slices (40%) (Wu & Raman, 2017). These results demonstrate that cfcEPSCs and mfEPSCs have distinct properties, and further suggest that electrical stimulation in slices primarily recruits mfEPSCs.

Given the composite nature of the EPSCs, we next applied the same analyses to measurements of charge transfer rather than peak amplitude. Charge transfer depressed to the same extent as amplitude ($P = 0.33$), suggesting that the dispersion of events within the response was replicable over sequential stimuli, and that these multiple events had similar short-term plasticity (P12–14, 0.47 ± 0.03, $n = 13$; P15–19, 0.50 ± 0.04, $n = 25$; ≥ P20, 0.49 ± 0.03, $n = 43$) (Fig. 2*E*). Together, these data demonstrate that, on average, synaptic transmission from IO neurons depresses equivalently in the cortex (Dittman & Regehr, 1998) and in the nuclei, regardless of the widely different synaptic innervation of individual Purkinje and CbN cells. These observations are in agreement with ultrastructural studies showing that both climbing fibres and their collaterals are filled with a high density of synaptic vesicles, unlike mossy fibres in the CbN, which have sparser synaptic vesicles (Chan Palay, 1977). Experimentally, the data also confirm that the stimulation of cfcEPSCs was probably not contaminated by mossy fibre inputs.

Effect of external calcium concentration on synaptic transmission

To test the extent to which cfcEPSC amplitudes, depression, and waveforms might be sensitive to calcium influx, we evoked synaptic currents in three concentrations of extracellular calcium: 1.5 mM (control), 0.5 mM ('low Ca') and 3 mM ('high Ca') (Fig. 3*A*). The magnesium concentration was adjusted to keep concentrations of divalent cations constant. Also, because NMDA receptors of CbN cells are only moderately blocked by magnesium (Audinat *et al.* 1990; Aizenman & Linden, 2000; Anchisi *et al.* 2001; Pugh & Raman, 2006), CPP was added to the bath to avoid changing the NMDAR contribution to cfcEPSCs. Since depression was equivalent across development, data from all ages ($n = 5$ and 4 cells from < P20 and ≥ P20 mice) were pooled in these experiments.

Low Ca decreased cfcEPSC amplitude to half its control value (normalized amplitude: 0.46 ± 0.06, $n = 8$, $P < 0.0001$, one-sample t test) (Fig. 3*B* and *C*) and increased the paired-pulse amplitude ratio from 0.48 ± 0.05 ($n = 9$) to 0.62 ± 0.06 ($n = 7$, $P = 0.025$) (Fig. 3*D*). By contrast, cfcEPSC amplitude was statistically unaffected by high Ca (normalized amplitude: 0.92 ± 0.04, $n = 10$, $P = 0.09$, one-sample t test) (Fig. 3*B* and *C*); nevertheless the paired-pulse ratio fell slightly but significantly to 0.40 ± 0.05 ($n = 9$, $P = 0.024$). Thus, release probability was not maximal in control solutions even though the postsynaptic response had apparently reached a ceiling (Fig. 3*D*). The overall effects of altering release probability via changing calcium concentration was similar to that reported at climbing fibre to Purkinje cell synapses for 5 Hz stimulation (Dittman & Regehr, 1998).

Mechanisms underlying composite cfcEPSCs

Notably, the composite waveforms of cfcEPSCs were retained in all concentrations of Ca. We therefore considered a series of possibilities that might give rise to multiple synaptic events occurring close enough in time to generate composite EPSCs. These include one or more of the following possibilities: (i) asynchronous release of vesicles within single boutons; (ii) differential coupling of release to calcium influx across different boutons; (iii) polysynaptic activation through the network of the cerebellar nuclei; (iv) different times to threshold for action potentials in multiple collaterals converging on one CbN cell; and (v) bursts of action potentials in single afferent collaterals.

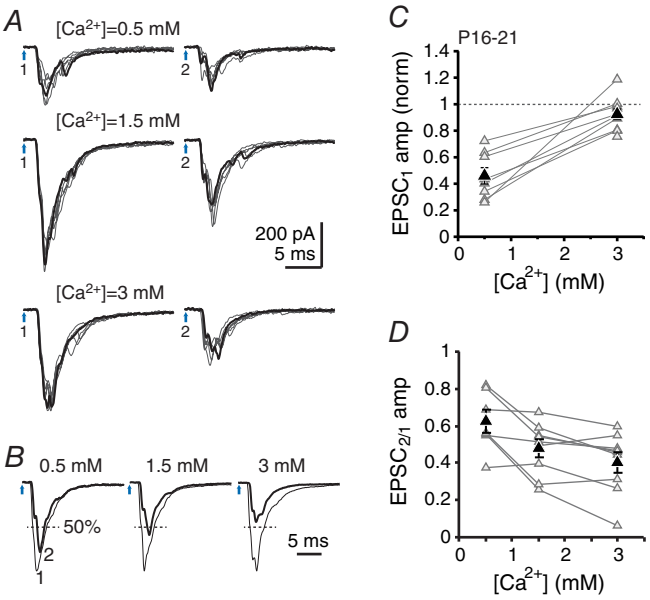

Figure 3. Effect of extracellular Ca concentration on cfcEPSC depression
A, cfcEPSCs evoked by a pair of light pulses (200 ms interval) for different concentrations of Ca. One example trace of six is highlighted. Blue arrows 1 and 2, stimulation times. *B*, superimposed normalized averages for $cfcEPSC_1$ and $cfcEPSC_2$. $cfcEPSC_2$ is highlighted. Dashed line indicates 50% of $EPSC_1$ amplitude. *C*, $cfcEPSC_1$ amplitude *vs.* Ca^{2+} concentration. Values are normalized to $cfcEPSC_1$ amplitude in control extracellular calcium (1.5 mM). *D*, paired-pulse amplitude ratio ($cfcEPSC_2/cfcEPSC_1$) *vs.* Ca concentration.

We began by analyzing the recordings in low Ca to assess the first and second possibilities for the basis for composite cfcEPSCs, namely, asynchronous release and/or differential coupling across boutons of vesicle fusion to calcium influx. In the former case, low Ca is expected to prolong the time course of release (Goda & Stevens, 1994; Atluri & Regehr, 1998). Similarly, in the latter case, reducing Ca influx might prolong the latency to fusion differentially across sites (Hefft & Jonas, 2005), which would decrease the peak current amplitude to a greater extent than the charge transfer. However, overlaying normalized averages of $cfcEPSC_1$ in control and low Ca precisely overlapped (Fig. 4*A*), and both peak current amplitude and charge transfer decreased equivalently in low Ca ($cfcEPSC_1$ charge transfer in low Ca, 0.50 ± 0.06, $n = 8$; $P = 0.3$) (Fig. 4*B* and *C*). Additionally, we calculated the ratio of the charge transfer within the first 2 ms relative to that in the first 4 ms ($cfcEPSC_{2ms/4\ ms}$) (Fig. 4*D*). This ratio was indistinguishable in low and control calcium, with values of 0.52 ± 0.06 and 0.56 ± 0.04, respectively ($n = 8$, $P = 0.15$). The stability of cfcEPSC waveforms across conditions that alter release probability means that asynchronous release or a diversity of calcium-to-release coupling probably does not account for the multiple peaks of cfcEPSCs.

The third possibility for composite EPSCs (i.e. polysynaptic activation) is probably also not responsible as a result of the short latencies (< 3 ms) of evoked cfcEPSCs. Nevertheless, to explore this idea further, we recorded cfcEPSCs at a holding potential of +50 mV in the presence of DNQX, aiming to block AMPAR-mediated excitatory synaptic transmission in the nuclei and limit the activation of other CbN neurons that could mediate a feed-forward excitation of the recorded cells. Gabazine was also included in the bath to block spontaneous IPSCs. Even under these conditions, light stimulation continued to reliably evoke short-latency NMDA cfcEPSCs (2.5 ± 0.2 ms, $n = 9$) (Fig. 4*E*). In four cells, further application of CPP blocked 97–100% of the cfcEPSC evoked in DNQX and gabazine. A double-exponential fit of the NMDAR cfcEPSC decay times gave a weighted decay time constant of 30 ± 6 ms, which did not vary consistently with age (Fig. 4*F*). The weighted time constant is more than twice the duration of electrically evoked, unitary NMDAR EPSCs in these cells (Wu & Raman, 2017), suggesting that the single peak results from the overlap of component cfcEPSCs. In general, the reliable nature and short latencies of these responses in DNQX indicate that climbing fibre collaterals directly activate large CbN neurons and suggest that the

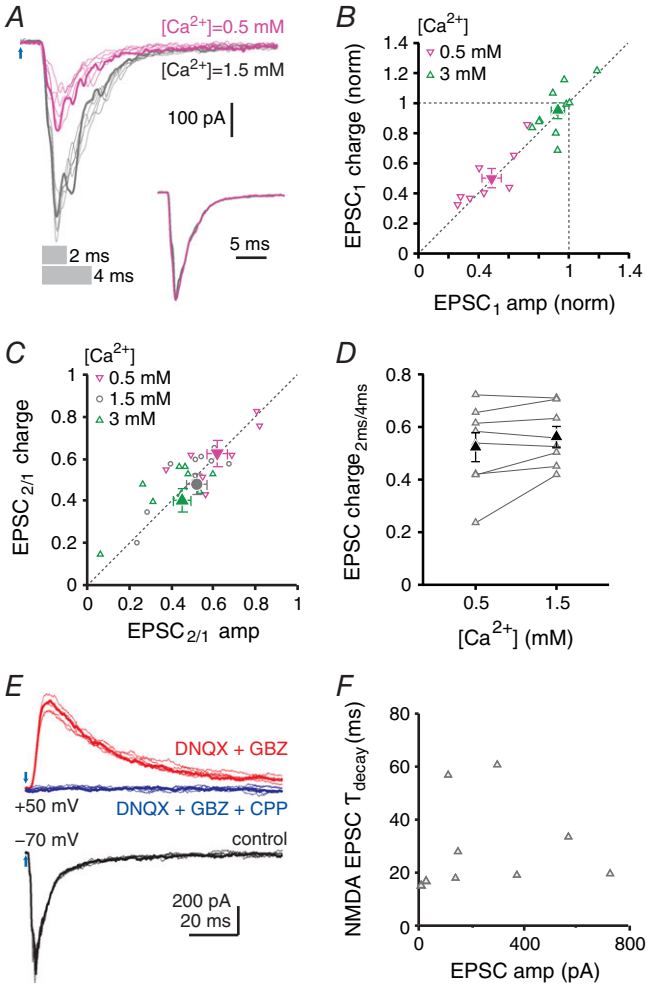

Figure 4. Composite cfcEPSCs are monosynaptic and independent of Ca concentration
A, cfcEPSCs recorded in control (grey traces) and low Ca (pink traces). Grey bars indicate the duration of the trace (2 ms or 4 ms) over which charge was calculated in (*D*). For each condition, one example trace of six is highlighted. Inset, superimposed normalized averages. *B*, cfcEPSC$_1$ charge *vs.* cfcEPSC$_1$ amplitude. Values are normalized to cfcEPSC$_1$ charge and amplitude in control Ca. Low Ca, 0.5 mM, downward pink triangles; high Ca, 3 mM, upward green triangles. Filled symbols are mean data. *C*, paired-pulse charge ratio *vs.* paired-pulse amplitude ratio. Low Ca, downward pink triangles; control Ca, grey circles; high Ca, upward green triangles. Filled symbols are mean data. *D*, relative charge transfer during the cfcEPSC, plotted as the ratio of charge transfer during the first 2 ms to the charge transfer during the first 4 ms *vs.* Ca^{2+} concentration (grey bars in *A*). *E*, example traces of control cfcEPSCs recorded at $V_{hold} = -70$ mV (black), the NMDA component isolated at $V_{hold} = +50$ mV after addition of DNQX (10 μM) and gabazine (10 μM) (red), and blockade of synaptic responses by further addition of CPP (10 μM) (blue). For each condition, one example trace among of six is highlighted. *F*, NMDAR cfcEPSC decay time constant (τ) *vs.* cfcEPSC amplitude. $V_{hold} = +50$ mV.

multiple peaks of composite EPSCs are monosynaptic in origin.

CbN cells receive inputs from convergent climbing fibre collaterals

Next, we investigated the fourth potential mechanism for composite cfcEPSCs, namely convergent inputs with different times to action potential threshold, by restricting activation to one or a few afferent fibres. To do so, we replaced the full-field illumination through the objective with local illumination through an optic fibre coupled to a cannula that targeted light onto the recorded cell and its immediate surroundings. 'Maximal' cfcEPSCs, from cells selected for their large amplitude responses, were initially recorded in response to the highest light intensity. The intensity was then reduced to the lowest intensity tested that still reliably evoked responses ('minimal suprathreshold' cfcEPSCs) (Fig. 5*A* and *B*) and, when possible, was decreased further to an intensity that evoked both failures and successes ('threshold' cfcEPSCs) (Fig. 5*C*). As the intensity was reduced from maximal to minimal suprathreshold, cfcEPSC amplitudes decreased tenfold, from 804 ± 122 pA to 78 ± 14 pA ($n = 18$, $P < 0.0001$) with a correspondingly large decrement in charge transfer, from 3.7 ± 0.7 nC to 0.26 ± 0.067 nC ($P < 0.0001$). The latency between the light stimulus and the cfcEPSC also increased as expected for smaller presynaptic depolarizations producing longer times to action potential threshold. The number of detectable events per cfcEPSC fell from 3.7 ± 0.3 to 2.2 ± 0.2 per stimulation ($P = 0.007$) (Fig. 5*D*), suggesting that the multiple peaks of composite cfcEPSCs indeed arise in part from the recruitment of multiple afferents.

Nevertheless, in 11 out of 12 cells recorded, 40 ± 7% of responses still showed more than one peak at threshold (2.2 ± 0.1 peaks) (Fig. 5*C* and *E*). Thus, even when only one afferent was expected to be activated, cfcEPSCs could be multipeaked, motivating an exploration of presynaptic bursts. Additionally, although threshold cfcEPSCs had similar amplitudes across age groups (< P20, 53 ± 3 pA, $n = 6$; > P20, 46 ± 5, $n = 6$, $P = 0.2$), the charge transfer at threshold stimulation was larger for younger than older animals (< P20, 178 ± 21 pC, $n = 6$; > P20, 92 ± 14, $n = 6$, $P = 0.0066$) (Fig. 5*F*), as was true for cfcEPSCs evoked by full-field illumination in Fig. 1. To test whether the greater charge transfer at threshold was independent of the number of peaks, we averaged the threshold cfcEPSCs that had only a single peak for each cell and measured their amplitudes and weighted decay time constants from double exponential fits (Fig. 5*G*). The peak currents were indistinguishable (< P20, 53 ± 6 pA, $n = 5$; > P20, 50 ± 5, $n = 6$; $P = 0.6$). The decay times, however, fell from 1.8 ± 0.5 ms for mice < P20 to 0.9 ± 0.2 for mice > P20 ($P = 0.04$)

(Fig. 5*H*), suggesting that slower receptor kinetics or more asynchronously activated synaptic sites per afferent might contribute to the greater charge transfer in younger mice.

The ratio of maximal-to-threshold cfcEPSC charge transfer ranged from 10–75 (Fig. 5*I*), which provides an estimate of the number of collaterals that converged onto the cells from which we recorded. These values could be an underestimate if not all afferents are stimulated; they could also be an overestimate if optogenetic stimulation independently activated the one to six branches of a single afferent (Sugihara *et al.* 1996, 1999). If these errors cancel each other out, then a few dozen inputs may have been present. Because these cells were chosen for high amplitude responses, however, their convergence ratios were not necessarily representative of the full population. Therefore, to estimate the mean convergence for each age range, we linearly fitted the plot of convergence ratio *vs.* maximal EPSC charge transfer for P12–14 and > P20 mice and then interpolated the convergence value

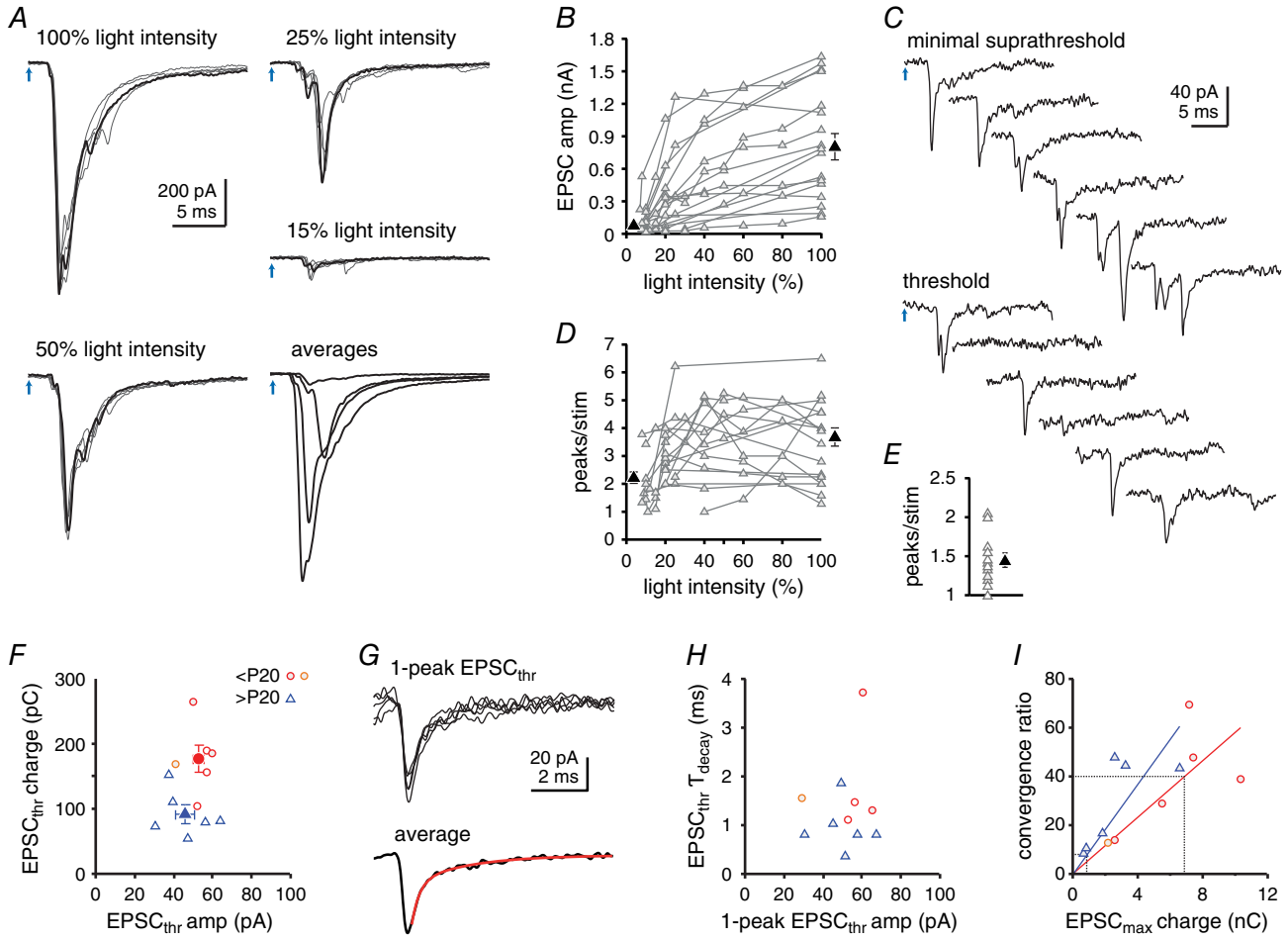

Figure 5. Convergence of multiple climbing fibre collaterals onto CbN cells
A, cfcEPSCs evoked by decreasing the intensity of stimulation through the optic fibre. For each light intensity, as labelled, one example trace of five is highlighted. Bottom right, superimposed averages of each intensity. All traces from same cell. *B*, cfcEPSC amplitude *vs.* light intensity for responses above threshold. Black filled symbols are averaged maximal amplitudes and averaged minimal suprathreshold amplitudes. *C*, threshold responses for stimulation evoking both successes and failures, and minimal suprathreshold responses. Six example traces. *D*, number of peaks per stimulation *vs.* light intensity for cfcEPSCs above threshold. Black filled symbols are mean number of peaks for maximal and minimal suprathreshold cfcEPSCs. *E*, number of peaks per threshold stimulation for successes only (threshold EPSC, $EPSC_{thr}$). Black filled symbol is the mean. *F*, threshold cfcEPSC charge transfer *vs.* cfcEPSC amplitude. Ages P12–14, red circles, P16, orange circles, > P20, blue triangles. Filled symbols are means. *G*, aligned traces of $cfcEPSC_{thr}$ that contained only one discernible peak. Top, five superimposed raw traces. Bottom, averaged trace with exponential fit (red). *H*, one-peak $cfcEPSC_{thr}$ decay time constant (τ) *vs.* $cfcEPSC_{thr}$ amplitude. Symbols as in (*F*). *I*, convergence ratio (max/threshold charge transfer) *vs.* charge transfer of maximal cfcEPSC. Symbols as in (*F*). Coloured lines are linear fits constrained to the origin for P12–14 (red) and > P20 (blue). Grey lines are interpolations of convergence ratios from mean EPSC charge transfer measured in Fig. 1.

corresponding to the mean charge transfer that we had previously measured for each population (Fig. 5*I*). For the juvenile group, the mean charge transfer (6.9 nC) predicted a convergence of 40 inputs and, for the older group, the mean charge transfer (0.9 nC) predicted a convergence of eight inputs. This analysis provides evidence that the number of climbing fibre afferents decreases over development.

Optogenetic stimulation of climbing fibre collaterals can elicit axonal bursts

Finally, we tested the fifth possibility for the presence of composite cfcEPSCs, namely, presynaptic action potential bursts. Recordings in the IO have demonstrated that olivary axons fire bursts of action potentials (Mathy *et al.* 2009). Indeed, composite EPSCs have been observed *in vivo* in Purkinje cells (Eccles *et al.* 1966; Amstrong & Rawson, 1979; Maruta *et al.* 2007; Mathy *et al.* 2009). Electrical and optogenetic stimulation of climbing fibres *in vitro* evoke only a single giant EPSC in Purkinje cells. By contrast, the persistence of multipeaked cfcEPSCs with threshold and minimal suprathreshold stimulation suggests that direct optogenetic activation can generate such bursts in the CbN. To address this possibility directly, we made loose-cell-attached recordings from IO axons in the cerebellar nuclei and in the cerebellar cortex for comparison.

In mice < P20, in response to either a maximal or submaximal light intensity, 42% of IO axons fired bursts of action potentials on a subset of trials (CbN, $n = 6$ out of 11; cortex, $n = 5$ out of 15, in the presence of DNQX) (Fig. 6*A* and *B*), whereas the remainder always fired a single action potential. This proportion decreased in older mice, with 26% of IO axons firing bursts (CbN, $n = 3$ out of 9; cortex, $n = 2$ out of 10) (Fig. 6*B*). Pooling ages, presynaptic action potential bursts were encountered in more collaterals than climbing fibres themselves, with 45% of axons in the CbN showing bursts ($n = 9$ out of 20) *vs.* 28% in the cortex ($n = 7$ out of 25) (Fig. 6*B*). Across ages and regions, in axons that fired bursts on at least one trial, the mean number of spikes was 2.3 ± 0.2 ($n = 16$). The observation that bursts varied consistently across cells, ages and cerebellar regions suggests that they were not an inevitable outcome of ChR2 expression, although they more probably reflect real differences in excitability of axons. Thus, burst firing decreases with development.

If the bursts are an artefact of oversized ChR2 currents, however, cells with more bursts might also be expected to have shorter latencies to fire. The latency of the first evoked spike was similar in axons with a tendency to burst (CbN, 1.2 ± 0.2 ms, $n = 9$; cortex, 0.5 ± 0.1 ms, $n = 7$) and axons firing a single action potential on every trial (CbN, 1.2 ± 0.4 ms, $n = 11$, $P = 0.2$; cortex, 0.5 ± 0.1 ms, $n = 18$, $P = 0.9$), suggesting that bursts are unlikely to be an artefact of ChR2 expression. Thus, the presence of multiple action potentials occurring at different times in multiple afferents appears to account for the composite nature of cfcEPSCs.

To compare the latencies of presynaptic spikes and EPSCs in the cortex and nuclei, the same axons were tested with maximal stimulus intensity applied through the objective. The latency of evoked axonal spikes was similar in both regions (CbN, 0.9 ± 0.2 ms, $n = 20$; cortex, 0.5 ± 0.1 ms, $n = 25$; $P = 0.16$), although the latency had a higher jitter in the CbN (CbN, 0.090 ± 0.041 ms; cortex 0.027 ± 0.002 ms; $P = 0.002$). Comparing the distributions of spike latencies and jitter showed that 15% of collaterals had latencies longer than 1.5 ms, whereas all climbing fibre latencies were shorter than 1.5 ms (Fig. 6*C*). In this regard, the presynaptic spike latencies differ from the postsynaptic currents, which had similar latencies in Purkinje and CbN cells (all ages collapsed). Moreover, 15% of climbing fibre collaterals had jitter values > 0.1 ms, whereas all climbing fibres had jitter values < 0.1 ms (Fig. 6*D*). Thus, it appears that CbN cells receive convergent inputs from collaterals with variable latencies, contributing further to temporal spread of cfcEPSCs.

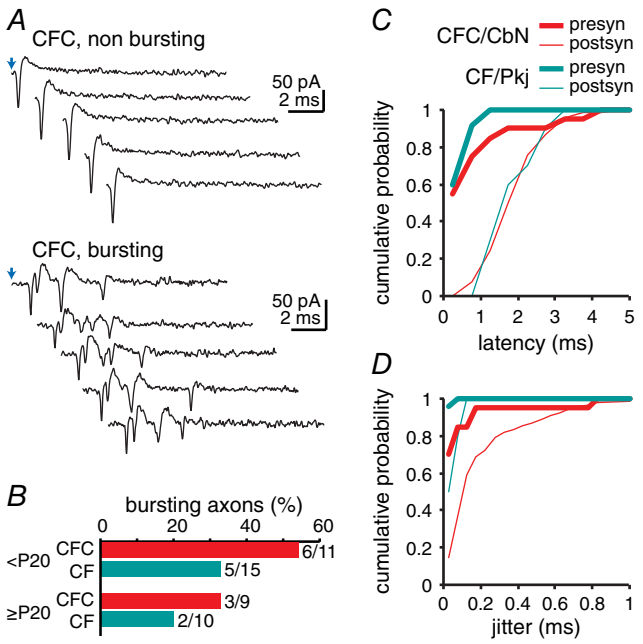

Figure 6. Climbing fibre and climbing fibre collateral axonal firing patterns evoked by light stimulation
A, loose-cell attached recording of fluorescent climbing fibre collateral axons. Top, five example traces from a non-burst-firing axon. Bottom, five example traces from a burst-firing axon. *B*, proportion of climbing fibre collateral (CFC, red) and climbing fibre (CF, blue) burst-firing axons at ages below and above P20. *C*, distribution of mean response latencies presynaptically (thick lines) and postsynaptically (thin lines) in the CbN (red) and in the cerebellar cortex (blue). *D*, same as (*C*) for jitter.

Effects of synaptic activation of climbing fibre collaterals on CbN cell action potentials

Because cfcEPSCs could be large, especially in younger animals, we tested their effect on CbN cell firing patterns in cell-attached recordings (Fig. 7*A*). Activating climbing fibre collaterals increased firing rates from a baseline of 56 ± 6 Hz to a maximal instantaneous frequency of 269 ± 42 Hz immediately after stimulation ($n = 21$, $P < 0.0001$) (Fig. 7*B* and *C*). In mice < P30, the first evoked spike had a latency of 3.3 ± 0.4 ms ($n = 16$) and a jitter of 0.68 ± 0.28 ms, giving a 0.83 ± 0.07 probability of spike occurrence during the 2–4 ms time window just after stimulation (Fig. 7*D*). To quantify the duration of the increase in firing probability, the PSTH was fitted with an exponential from the peak number of spikes per bin to the steady value associated with spontaneous firing. Consistent with the larger charge-to-amplitude ratio reported for cfcEPSCs, the effect of climbing fibre collateral activation lasted longer at P12–14 (11.7 ± 1.9 ms, $n = 5$) than at P15–19 (5.5 ± 1 ms, $n = 5$, $P = 0.04$) or at P20–30 (2.2 ± 1 ms, $n = 5$, $P = 0.005$) (Fig. 7*E*). This analysis therefore suggests that climbing fibre collateral inputs can have brief but large effects on CbN cell firing in mice during the first month of postnatal life.

Discussion

These experiments demonstrate that climbing fibre collaterals, which carry a copy of the instructive signals transmitted to the cerebellar cortex from the IO, provide strong synaptic input to large CbN cells early in postnatal development and also that the total magnitude of this input is reduced with age. Their terminals retain a high release probability throughout development and a constant threshold response, although the number of collaterals contacting each CbN cell decreases. The convergence of tens of afferents with different times to spike threshold, among which a subset fires bursts of action potentials, results in EPSCs with multiple peaks. At least through the first postnatal month, activation of these synapses can evoke well-timed increases in firing probability. Together, these results indicate that climbing fibre collaterals probably exert their strongest functional effect early in postnatal development, over the same period during which climbing fibres of the cortex are being pruned, suggestive of a role in the wiring of potentially closed-loop cerebellar circuits.

Comparison with mossy fibre inputs

Although Purkinje cells constitute the majority of synaptic input to large CbN cells, accounting for 86% of somatic and 50% of dendritic synapses, CbN neurons also receive glutamatergic input from mossy fibres and climbing fibre collaterals, which form 22% and 5%, respectively, of synapses onto proximal dendrites (Chan-Palay, 1977; Palkovits *et al.* 1977; De Zeeuw & Berrebi, 1995). Based on the four- to five-fold difference in the number of contacts, EPSCs evoked *in vitro* by electrical stimulation of the white matter surrounding large CbN neurons have been attributed to mossy fibres (Pugh & Raman, 2006; Zhang & Linden, 2006; Person & Raman, 2010). The present data suggest that, because climbing fibre collateral inputs can have large amplitudes, especially early in life, these studies may well have included cfcEPSCs. The extent of depression for electrically evoked EPSCs, however, is much lower than for cfcEPSCs and instead resembles that of optically isolated mfEPSCs. The simplest explanation for this result is that mossy fibres are more readily activated by electrical stimulation in slices. When climbing

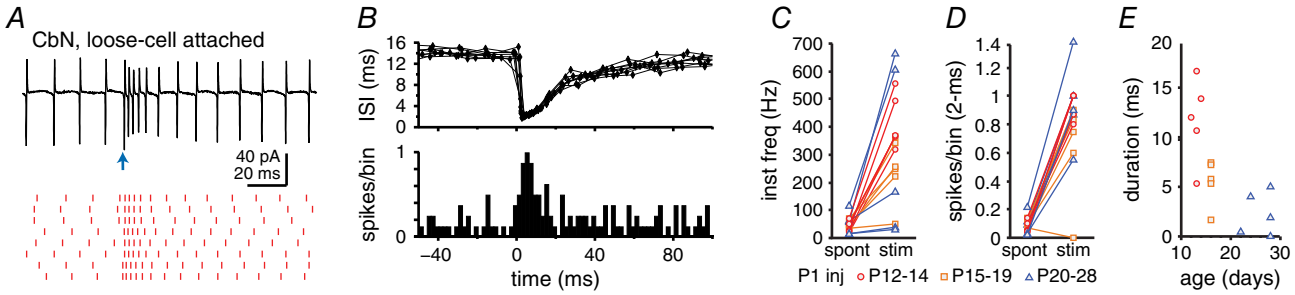

Figure 7. Effects of climbing fibre collateral inputs on CbN cell firing rate and timing
A, loose-cell attached recording of a CbN neuron (P13). Top, single raw trace. Bottom, raster plot of eight trials. *B*, top, interspike interval duration (ISI) *vs.* time. Eight superimposed traces. Black lozenges show spike timing. Bottom, PSTH of spike probability (2 ms bin) *vs.* time. Same cell as in (*A*). *C*, immediate effect of cfcEPSC stimulation on rate, plotted as mean instantaneous firing rate during the 500 ms preceding stimulation (spont) and for the first interspike interval after the stimulation (stim). *D*, immediate effect of cfcEPSC stimulation on spike timing, plotted as mean spike probability (in 2 ms bins) during the 500 ms preceding the stimulation (spont) and during the 2–4 ms time window after the stimulation (stim). *E*, duration of the increase in firing rate induced by cfcEPSC stimulation, measured from a single-exponential fit to the decay of the PSTH of spike probability (5 ms bins).

fibre collaterals are successfully stimulated, however, they elicit 'threshold' responses of ∼0.67 nS (∼50 pA with a driving force of ∼74 mV), which is approximately two-thirds the magnitude of electrically evoked unitary EPSCs, probably arising from mossy fibres (Wu & Raman, 2015).

The strong depression of cfcEPSCs is consistent with a high release probability, similar to that of climbing fibre synapses onto Purkinje cells (Eccles *et al.* 1966; Dittman & Regehr, 1998; Hashimoto & Kano, 1998; Silver *et al.* 1998). This physiological similarity parallels an ultrastructural similarity, namely that inferior olivary boutons are filled with densely packed vesicles in both the cortex and the nuclei (Chan Palay, 1977). By contrast, mossy fibre inputs to the nuclei had paired-pulse ratios close to 0.75 (5 Hz), resembling that of mossy fibre inputs onto granule cells (∼0.8 at 5–10 Hz) (Xu-Friedman & Regehr, 2003). Thus, despite the great disparity between inferior olivary axonal arborizations in the cortex and nuclei, climbing fibres and their collaterals share physiological properties at the level of individual synapses, which distinguish them from mossy fibres.

Presynaptic contributions to EPSC waveform

A distinctive attribute of cfcEPSCs was their composite nature. Investigating the underlying mechanisms demonstrated that these multipeaked waveforms resulted in part from bursts of action potentials in the presynaptic axons. Interestingly, brief optogenetic depolarization solely of axons triggered bursts more frequently in collaterals than in climbing fibres themselves. This difference may reflect a higher excitability of axons in the nuclei as a result of the thinner branches of the collaterals (van der Want *et al.* 1989; Sugihara *et al.* 1996) or differences in ion channel properties and/or localization.

In intact preparations, rhythmic subthreshold oscillations in the somata of inferior olivary neurons give rise to bursts of axonal action potentials (Mathy *et al.* 2009). The transmission of these bursts is of interest because recent work suggests that they can be informationally rich. In the cerebellar cortex, propagated bursts elicit multiple climbing fibre EPSPs, which can increase the number of spikelets in Purkinje cell complex spikes (Eccles *et al.* 1966; Amstrong & Rawson, 1979; Maruta *et al.* 2007; Mathy *et al.* 2009). The duration of complex spikes, in turn, can distinguish spontaneous and sensory-evoked events (Maruta *et al.* 2007; Najafi & Medina, 2013) and correlates with the magnitudes of synaptic plasticity and learned responses (Mathy *et al.* 2009; Yang & Lisberger, 2014). The present data therefore suggest that CbN cells, too, may receive graded information from the IO.

Climbing fibre collateral properties through development

Previous studies have examined the magnitude of cfcEPSPs at different ages. Extracellular recordings in the rat interpositus suggested slight increases in the early phase of the field potential evoked by electrical stimulation of the IO in P24 *vs.* P17 rats (Nicholson & Freeman, 2004), whereas a previous study of the physiological effects of climbing fibre collateral activity on CbN cells in 3–6-month-old mice reported EPSCs of ∼7 pA or EPSPs of 1-2 mV in five of 13 cells that responded to optogenetic stimulation of ChR2-expressing afferents (Lu *et al.* 2016). These small responses are consistent with the developmental decrease in the strength of this pathway in the present study. However, we also observed that, although cfcEPSC amplitudes fell from > 1 nA at the end of the second postnatal week to a few hundred pA by the end of the third week, the responses then remained constant until mice were ∼2 months old. It is possible that a second phase of diminution of the response occurs during the third postnatal month. Alternatively, the studies could differ in the nature of ChR2 expression. Because IO neurons express Ptf1a only during embryogenesis (Yamada *et al.* 2007), the level of Ptf1a-dependent ChR2 expression in inferior olivary neurons might have decreased during postnatal life, leaving only a subset of existing climbing fibre collaterals capable of being readily activated optogenetically. Nevertheless, both studies are consistent with the idea that the strength of climbing fibre collaterals is lower in adults than in juveniles. However, it is worth noting that the role of climbing fibre collaterals to the CbN need not be exclusively developmental because they can provide inputs to CbN cells of a few hundred pA at −70 mV well into the second month of life. Given the role of IO signals in instructing plasticity in the cerebellar cortex, the climbing fibre collaterals could provide either electrical or biochemical signals to the CbN that modulate or intensify this plasticity, as has been suggested by modelling studies (Luque et al. 2014).

Possible contributions of climbing fibre collaterals to circuit formation

An interesting proposal is that activity of climbing fibre collaterals may participate in the wiring of the cerebellar circuit (Lu *et al.* 2016; Lang *et al.* 2017), possibly when the pruning of climbing fibres occurs in the cerebellar cortex (Crépel *et al.* 1976; Hashimoto & Kano, 2003; Sugihara, 2006). Such a developmental role might include the formation of closed loops, in which the Purkinje cell targeted by a specific IO cell would form synapses onto the CbN cell receiving collaterals from the same IO cell (Voogd & Bigaré, 1980; Ruigrok & Voogd, 2000; Apps & Hawkes, 2009; Ruigrok, 2010; Sugihara, 2011; Cerminara

et al. 2013). In the mature cerebellar cortex, a single IO cell gives rise to approximately seven climbing fibres, each contacting one Purkinje cell (Sugihara *et al.* 1999), and ∼30–50 Purkinje cells converge onto each large CbN cell (Person & Raman, 2012). If these Purkinje cells were innervated by different IO cells, then the climbing fibre collateral convergence onto a CbN cell would also be 30–50 in a closed-loop circuit. If, however, a given IO cell contacted seven Purkinje cells that converged in the nuclei, then the number of climbing fibre collateral inputs predicted to form synapses onto a CbN cell in a closed loop would fall to ∼4–7.

The present data suggest that a single juvenile CbN cell receives input from ∼40 IO cells. However, it is difficult to infer the likelihood of closed loops at young ages because, at ≤ P21, Purkinje cells can receive input from multiple climbing fibres. After P21, however, each Purkinje cell is innervated by only one climbing fibre and the results of the present study indicate that each CbN cell receives input from approximately eight collaterals, a value near the 4–7 predicted for the closed loop scenario. Specifically, each of these eight collaterals would emerge from an equal number of IO cells, each of which would contact approximately seven Purkinje cells. Approximately 56 Purkinje cells would therefore be within the loop, which is in the range of the number of Purkinje cells expected to converge onto a CbN cell.

Such a scenario predicts that climbing fibre collateral excitation would be immediately followed by inhibition from approximately seven Purkinje afferents. Given the temporal dispersion of individual cfcEPSCs and the lower total excitatory *vs.* inhibitory conductance (Person & Raman, 2012), it is possible that dendritic filtering *in vivo* could make inhibition overwhelm any preceding excitation even when it is present. Nevertheless, at a biochemical and/or structural level, if synaptic inputs to CbN cells were stabilized during development by a combination of cfcEPSPs preceding coincident IPSPs from multiple afferents, then the circuit would be able to select for Purkinje cells that allow the formation of closed loops.

References

Aizenman CD & Linden DJ (2000). Rapid, synaptically driven increases in the intrinsic excitability of cerebellar deep nuclear neurons. *Nat Neurosci* **3**, 109–111.

Albus JS (1971). A theory of cerebellar function. *Math Biosci* **10**, 25–61.

Anchisi D, Scelfo B & Tempia F (2001). Postsynaptic currents in deep cerebellar nuclei. *J Neurophysiol* **85**, 323–331.

Armstrong DM & Rawson JA (1979). Activity patterns of cerebellar cortical neurones and climbing fibre afferents in the awake cat. *J Physiol* **289**, 425–448.

Apps R & Hawkes R (2009). Cerebellar cortical organization: a one-map hypothesis. *Nat Rev Neurosci* **10**, 670–681.

Atluri PP & Regehr WG (1998). Delayed release of neurotransmitter from cerebellar granule cells. *J Neurosci* **18**, 8214–8227.

Audinat E, Knöpfel T & Gähwiler BH (1990). Responses to excitatory amino acids of Purkinje cells and neurones of the deep nuclei in cerebellar slice cultures. *J Physiol* **430**, 297–313.

Blenkinsop TA & Lang EJ (2011). Synaptic action of the olivocerebellar system on cerebellar nuclear spike activity. *J Neurosci* **31**, 14708–14720.

Cerminara NL, Aoki H, Loft M, Sugihara I & Apps R (2013). Structural basis of cerebellar microcircuits in the rat. *J Neurosci* **33**, 16427–16442.

Chan-Palay V (1977). *Cerebellar Dentate Nucleus: Organization, Cytology, and Transmitters*. Springer, Berlin, pp. 126, 275–280, 282.

Crépel F, Mariani J & Delhaye-Bouchaud N (1976). Evidence for a multiple innervation of Purkinje cells by climbing fibers in the immature rat cerebellum. *J Neurobiol* **7**, 567–578.

De Zeeuw CI & Berrebi AS (1995). Postsynaptic targets of Purkinje cell terminals in the cerebellar and vestibular nuclei of the rat. *Eur J Neurosci* **7**, 2322–2333.

De Zeeuw CI, Van Alphen AM, Hawkins RK & Ruigrok TJ (1997). Climbing fibre collaterals contact neurons in the cerebellar nuclei that provide a GABAergic feedback to the inferior olive. *Neuroscience* **80**, 981–986.

Dittman JS & Regehr WG (1998). Calcium dependence and recovery kinetics of presynaptic depression at the climbing fiber to Purkinje cell synapse. *J Neurosci* **18**, 6147–6162.

Eccles JC, Llinás R & Sasaki K (1966). The excitatory synaptic action of climbing fibres on the Purkinje cells of the cerebellum. *J Physiol* **182**, 268–296.

Eccles JC, Sabah NH & Táboríková H (1974). The pathways responsible for excitation and inhibition of fastigial neurones. *Exp Brain Res* **19**, 78–99.

García KS & Mauk MD (1998). Pharmacological analysis of cerebellar contributions to the timing and expression of conditioned eyelid responses. *Neuropharmacology* **37**, 471–480.

Gilbert PF & Thach WT (1977). Purkinje cell activity during motor learning. *Brain Res* **128**, 309–328.

Goda Y & Stevens CF (1994). Two components of transmitter release at a central synapse. *Proc Natl Acad Sci USA* **91**, 12942–12946.

Grundy D (2015). Principles and standards for reporting animal experiments in *The Journal of Physiology* and *Experimental Physiology*. *J Physiol* **593**, 2547–2549.

Hashimoto K & Kano M (1998). Presynaptic origin of paired-pulse depression at climbing fibre-Purkinje cell synapses in the rat cerebellum. *J Physiol* **506**, 391–405.

Hashimoto K & Kano M (2003). Functional differentiation of multiple climbing fiber inputs during synapse elimination in the developing cerebellum. *Neuron* **38**, 785–796.

Hefft S & Jonas P (2005). Asynchronous GABA release generates long-lasting inhibition at a hippocampal interneuron-principal neuron synapse. *Nat Neurosci* **8**, 1319–1328.

Khosrovani S, Van Der Giessen RS, De Zeeuw CI & De Jeu MT (2007). In vivo mouse inferior olive neurons exhibit heterogeneous subthreshold oscillations and spiking patterns. *Proc Natl Acad Sci USA* **104**, 15911–15916.

Konnerth A, Llano I & Armstrong CM (1990). Synaptic currents in cerebellar Purkinje cells. *Proc Natl Acad Sci USA* **87**, 2662–2665.

Lang EJ, Sugihara I, Welsh JP & Llinás R (1999). Patterns of spontaneous Purkinje cell complex spike activity in the awake rat. *J Neurosci* **19**, 2728–2739.

Lang EJ, Apps R, Bengtsson F, Cerminara NL, De Zeeuw CI, Ebner TJ, Heck DH, Jaeger D, Jörntell H, Kawato M, Otis TS, Ozyildirim O, Popa LS, Reeves AM, Schweighofer N, Sugihara I & Xiao J (2017). The roles of the olivocerebellar pathway in motor learning and motor control. A consensus paper. *Cerebellum* **16**, 230–252.

Llinás R & Mühlethaler M (1988). Electrophysiology of guinea-pig cerebellar nuclear cells in the in vitro brain stem-cerebellar preparation. *J Physiol* **404**, 241–258.

Llinás R & Sasaki K (1989). The functional organization of the olivo-cerebellar system as examined by multiple Purkinje cell recordings. *Eur J Neurosci* **1**, 587–602.

Lu H, Yang B & Jaeger D (2016). Cerebellar nuclei neurons show only small excitatory responses to optogenetic olivary stimulation in transgenic mice: in vivo and in vitro studies. *Front Neural Circuits* **10**, 21.

Luque NR, Garrido JA, Carrillo RR, D'Angelo E & Ros E (2014). Fast convergence of learning requires plasticity between inferior olive and deep cerebellar nuclei in a manipulation task: a closed-loop robotic simulation. *Front Comput Neurosci* **8**, 97.

Marr D (1969). A theory of cerebellar cortex. *J Physiol* **202**, 437–470.

Maruta J, Hensbroek RA & Simpson JI (2007). Intraburst and interburst signaling by climbing fibers. *J Neurosci* **27**, 11263–11270.

Mathy A, Ho SS, Davie JT, Duguid IC, Clark BA & Häusser M (2009). Encoding of oscillations by axonal bursts in inferior olive neurons. *Neuron* **62**, 388–399.

Medina JF, Nores WL & Mauk MD (2002). Inhibition of climbing fibres is a signal for the extinction of conditioned eyelid responses. *Nature* **416**, 330–333.

Mercer AA, Palarz KJ, Tabatadze N, Woolley CS & Raman IM (2016). Sex differences in cerebellar synaptic transmission and sex-specific responses to autism-linked Gabrb3 mutations in mice. *Elife* **5**, e07596.

Miyashita T, Shao YR, Chung J, Pourzia O & Feldman DE (2013). Long-term channelrhodopsin-2 (ChR2) expression can induce abnormal axonal morphology and targeting in cerebral cortex. *Front Neural Circuits* **7**, 8.

Najac M & Raman IM (2015). Integration of Purkinje cell inhibition by cerebellar nucleo-olivary neurons. *J Neurosci* **35**, 544–549.

Najafi F & Medina JF (2013). Beyond 'all-or-nothing' climbing fibers: graded representation of teaching signals in Purkinje cells. *Front Neural Circuits* **7**, 115.

Nguyen-Vu TD, Kimpo RR, Rinaldi JM, Kohli A, Zeng H, Deisseroth K & Raymond JL (2013). Cerebellar Purkinje cell activity drives motor learning. *Nat Neurosci* **16**, 1734–1736.

Nicholson DA & Freeman JH Jr (2004). Selective developmental increase in the climbing fiber input to the cerebellar interpositus nucleus in rats. *Behav Neurosci*, **118**, 1111–1116.

Palkovits M, Mezey E, Hámori J & Szentágothai J (1977). Quantitative histological analysis of the cerebellar nuclei in the cat. I. Numerical data on cells and on synapses. *Exp Brain Res* **28**, 189–209.

Person AL & Raman IM (2010). Deactivation of L-type Ca current by inhibition controls LTP at excitatory synapses in the cerebellar nuclei. *Neuron* **66**, 550–559.

Person AL & Raman IM (2012). Purkinje neuron synchrony elicits time-locked spiking in the cerebellar nuclei. *Nature* **481**, 502–505.

Pugh JR & Raman IM (2006). Potentiation of mossy fiber EPSCs in the cerebellar nuclei by NMDA receptor activation followed by postinhibitory rebound current. *Neuron* **51**, 113–123.

Rahimi-Balaei M, Afsharinezhad P, Bailey K, Buchok M, Yeganeh B & Marzban H (2015). Embryonic stages in cerebellar afferent development. *Cerebellum Ataxias* 2:7. https://doi.org/10.1186/s40673-015-0026-y.

Ruigrok TJ & Voogd J (2000). Organization of projections from the inferior olive to the cerebellar nuclei in the rat. *J Comp Neurol* **426**, 209–228.

Silver RA, Momiyama A & Cull-Candy SG (1998). Locus of frequency-dependent depression identified with multiple-probability fluctuation analysis at rat climbing fibre-Purkinje cell synapses. *J Physiol* **510**, 881–902.

Sugihara I, Wu H & Shinoda Y (1996). Morphology of axon collaterals of single climbing fibers in the deep cerebellar nuclei of the rat. *Neurosci Lett* **217**, 33–36.

Sugihara I, Wu H & Shinoda Y (1999). Morphology of single olivocerebellar axons labeled with biotinylated dextran amine in the rat. *J Comp Neurol* **414**, 131–148.

Sugihara I, Wu H & Shinoda Y (2001). The entire trajectories of single olivocerebellar axons in the cerebellar cortex and their contribution to cerebellar compartmentalization. *J Neurosci* **21**, 7715–7723.

Sugihara I (2005). Microzonal projection and climbing fiber remodeling in single olivocerebellar axons of newborn rats at postnatal days 4–7. *J Comp Neurol* **487**, 93–106.

Sugihara I (2006). Organization and remodeling of the olivocerebellar climbing fiber projection. *Cerebellum* **5**, 15–22.

Sugihara I (2011). Compartmentalization of the deep cerebellar nuclei based on afferent projections and aldolase C expression. *Cerebellum* **10**, 449–463.

Tang T, Suh CY, Blenkinsop TA & Lang EJ (2016). Synchrony is key: complex spike inhibition of the deep cerebellar nuclei. *Cerebellum* **15**, 10–13.

Thach WT (1968). Discharge of Purkinje and cerebellar nuclear neurons during rapidly alternating arm movements in the monkey. *J Neurophysiol* **31**, 785–797.

van der Want JJ & Voogd J (1987). Ultrastructural identification and localization of climbing fiber terminals in the fastigial nucleus of the cat. *J Comp Neurol* **258**, 81–90.

van der Want JJ, Wiklund L, Guegan M, Ruigrok T, Voogd J (1989). Anterograde tracing of the rat olivocerebellar system with Phaseolus vulgaris leucoagglutinin (PHA-L). Demonstration of climbing fiber collateral innervation of the cerebellar nuclei. *J Comp Neurol* **288**, 1–18.

Voogd J & Bigaré F (1980). Topographical distribution of olivary and cortico nuclear fibers in the cerebellum: a review. In *The Inferior Olivary Nucleus: Anatomy and Physiology*, eds Courville J, DeMontigny C & Lamarre Y. Raven Press, New York, NY.

Wadiche JI & Jahr CE (2001). Multivesicular release at climbing fiber-Purkinje cell synapses. *Neuron* **32**, 301–313.

Wiklund L, Toggenburger G & Cuénod M (1984). Selective retrograde labelling of the rat olivocerebellar climbing fiber system with D-[^{3}H]aspartate. *Neuroscience* **13**, 441–468.

Wu Y & Raman IM (2017). Facilitation of mossy fibre-driven spiking in the cerebellar nuclei by the synchrony of inhibition. *J Physiol* **595**, 5245–5264.

Xu-Friedman MA & Regehr WG (2003). Ultrastructural contributions to desensitization at cerebellar mossy fiber to granule cell synapses. *J Neurosci* **23**, 2182–2192.

Yamada M, Terao M, Terashima T, Fujiyama T, Kawaguchi Y, Nabeshima Y & Hoshino M (2007). Origin of climbing fiber neurons and their developmental dependence on Ptf1a. *J Neurosci* **27**, 10924–10934.

Yang Y & Lisberger SG (2014). Purkinje-cell plasticity and cerebellar motor learning are graded by complex-spike duration. *Nature* **510**, 529–532.

Zhang W & Linden DJ (2006). Long-term depression at the mossy fiber-deep cerebellar nucleus synapse. *J Neurosci* **26**, 6935–6944.

Additional information

Competing interests

The authors declare that they have no competing interests.

Author contributions

IMR and MN were responsible for the study conception, study design, interpretation of the data, drafting the manuscript and revision of the manuscript. MN performed the data acquisition and analysis. All authors approved the final manuscript, are accountable for the accuracy and integrity of the research, and are the only people qualified for authorship of the work.

Funding

Supported by the National Institutes of Health R37-NS39395 (IMR).

Acknowledgements

Confocal imaging was conducted in the Biological Imaging Facility of Northwestern University. We thank members of the Raman laboratory for helpful discussions and comments on the manuscript.